Method for calculating dynamic yield stress of fresh cement pastes using a coaxial cylinder system

Yiming Peng [1, 2], *Kunlin Ma* [1, *], *Cise Unluer* [2], *Wenxu Li* [1], *Shuangjie Li* [1], *Jinyan Shi* [1], *Guangcheng Long* [1]

[1] School of Civil Engineering, National Engineering Laboratory for High-speed Railway Construction, Central South University, Changsha 410075, China

[2] School of Engineering, University of Glasgow, Glasgow G12 8LT, United Kingdom

*Corresponding author at: School of Civil Engineering, National Engineering Laboratory for High-speed Railway Construction, Central South University, Changsha 410075, China

Abstract: The calculation of the rheological parameters of fresh cement pastes plays a key role in understanding the rheology of cement-based mixes. Because cement paste is not a simple Bingham fluid, a suitable nonlinear model must be found for characterizing its flow. A test system in which the rotational speed or shear rate can be changed in multiple steps is regarded as a suitable rheological test protocol because the paste reaches a steady state. Furthermore, theoretical derivations show that the solution of the Couette inverse problem corresponding to the modified Bingham model and the Herschel–Bulkley (H-B) model is complex. However, a comparative analysis revealed that the yield stress of fresh paste could easily be obtained through a calculation process based on a Parabolic model. This study presents the complete calculation procedure for this model. The influence of the plug flow is considered, and test points with low minimum shear stress (τ_{min}) are excluded. Finally, the accuracy of the proposed method is verified through comparisons with the results obtained using mini-cone slump tests. These results show that the dynamic yield stress calculated using the expression of the Couette inverse problem based on the Parabolic model in consideration of the plug flow is very close to the yield stress obtained using the mini-cone slump

flow test. This proves that the proposed method could precisely characterize the dynamic yield stress of cement pastes.

Keywords: cement paste; dynamic yield stress; Couette inverse problem; coaxial cylinders rheometer; plug flow

1. Introduction

Fresh cement mixes are multiscale, multiphase, solid–liquid dispersion systems [1]. The individual particles in these mixes undergo irregular Brownian motion, collisions, and friction, and they exhibit electrostatic repulsion and Van der Waals forces [2-4]. In terms of rheological properties, cement paste shows more plastic properties when it is fresh. With continuous hydration, the cement paste gradually loses its fluidity, sets, and hardens into a semisolid or solid-phase system dominated by viscoelasticity [5-6].

The rheological properties strongly influence the macroscopic working performance of fresh cement-based materials. This performance can be characterized by specific rheological models that represent a functional relationship (i.e., a constitutive equation) between the shear stress and the shear rate of the flowing material [7]. For example, in the commonly used Bingham model, the two basic rheological parameters are the yield stress and plastic viscosity [8-9]. Meanwhile, the rheological properties reflect the change in the viscosity of the cement paste with variations in the external shear force. When the first derivative value of the shear stress (i.e., the differential viscosity of the paste at a certain shear rate) increases with an increase in the shear rate, the paste exhibits

shear thickening behavior; by contrast, when the differential viscosity decreases with an increase in the shear rate, the paste exhibits shear thinning behavior [10]. The addition of certain chemical and mineral admixtures as well as changes in the ambient temperature and resting time may also influence the shear thickening or shear thinning behavior of the paste [8,11,12].

The shear stress and shear rate may have a nonlinear relationship. The Herschel–Bulkley (H-B) model and the modified Bingham model have been proposed to describe such nonlinear flow behaviors [13]. To relate these two models, the H-B model equation is expanded using the Taylor expansion at a certain shear rate a [14]. Then, by dividing the shear rate terms $\dot{\gamma}$ and $\dot{\gamma}^2$ of both the expanded equation and the modified Bingham model, a functional relationship between c/μ and n is obtained, and a relationship between the shear thickening coefficients of the two models is established. However, with the addition of different types of admixtures, the phase compositions of the composite pastes become increasingly complex. The rheological characteristics of the paste gradually change with an increase in the shear rate (i.e., shear thickening or shear thinning is not observed in the shear test), making it challenging to determine a specific and suitable rheological model for characterizing the rheological parameters [15-17].

Cement paste can resist an external shear force and not flow. This resistance, defined as the yield stress, arises from the microcosmic network structure formed by colloidal interactions [18-20], and it depends on the strength and structure of this network in the cement paste [21,22]. When cement paste is in a static state, colloidal flocculation and cement hydration bonding (e.g., C-S-H bridge) densify its microstructure, thus increasing the yield stress [18,23]. Under shear forces, this

microstructure can break down and thereby reduce the yield stress. Therefore, from the perspective of two different initial states, the yield stress can be further divided into static and dynamic yield stress [24, 25]. The static yield stress is the minimum stress required to initiate the flow of the paste, and it corresponds to the state of the microstructure before it breaks down. The dynamic yield stress is the minimum stress required to maintain the flow behavior, during which the internal microstructure of the paste is modified.

The difference in the yield stress of fresh cement pastes between the rest and the flow states is referred to as thixotropy [26-28]. In rheology, thixotropic behavior is defined as a time-dependent parameter that represents the decrease in structural strength under the action of a constant shear force followed by the recovery of the structure to its original state during a subsequent resting process [21,29,30]. The process of structural damage and recovery is a completely reversible cycle, and it is most commonly characterized by the thixotropic loop area and the three-interval thixotropy test (3ITT) methods [31-35]. A previous study [36] showed that a new equilibrium flow state can be established for a thixotropic fluid only after a constant shear rate is imposed for a certain duration. Therefore, the method of multiple step changes in shear rate was proposed to quantitatively evaluate the thixotropy. As shown in **Fig. 1**, this method involves measuring the tangential stress and viscosity at different times at a constant shear rate until the tangential stress gradually reaches equilibrium [36]. A function of the shear stress and viscosity with time can be obtained through repeated measurements under different shear rates to evaluate both the thixotropy and the time-dependent rheology of cement pastes in a steady flow state.

In a coaxial cylinder system, a rheometer can be used to reveal the relationship between the rotational velocity (N) and the torque (T). The conversion of the N–T relation obtained using the rheometer into the parameters of a specific rheological model, namely, the shear stress (τ) and shear rate ($\dot{\gamma}$), has long remained a fundamental challenge in rheology calculations and has given rise to the famous Couette inverse problem [37, 38]. Rheometers can not only measure test points with different T and N but also automatically calculate their corresponding τ and $\dot{\gamma}$. From the results obtained using the rheometer, the intercept of different rheological models (i.e., Bingham model, H-B model, and modified Bingham model), namely, the dynamic yield stress, can be obtained. However, most rheometers use only semiempirical methods to solve the Couette inverse problem instead of complete mathematical and mechanical derivations. Therefore, several studies have aimed to develop solutions for the Couette inverse problem based on these rheological models [39-41].

The solution of the Bingham model is calculated using the widely used and validated Reiner–Riwlin equation [42]. However, the solutions of the modified Bingham model and H-B model remain controversial. Feys et al. [39] studied the solution of the Couette inverse problem based on the modified Bingham model under the condition of a coaxial cylinder test system. By contrast, Heirman et al. [40] calculated the solution of the Couette inverse problem based on the H-B model. However, a subsequent theoretical analysis [41] indicated that the derivations in the above two studies contained major errors. Choosing a suitable rheological model to derive the solution of the Couette inverse problem and accurately calculating the rheological parameters remain important challenges that must be overcome for better understanding the rheology of cement mixes.

Cement mixes have complex compositions, and therefore, the applicability of existing rheological models to reveal the rheological properties of fresh cement mixes having different compositions needs to be further investigated. In this light, the present study aims to identify and propose an accurate method for calculating the dynamic yield stress of fresh cement pastes under a coaxial cylinder system. In consideration of the effect of a plug flow, a Parabolic model is used instead of the H-B model and modified Bingham model for performing calculations. A coaxial cylinder rheometer is applied to test the steady-state rheological properties of cement mixes having different mixture proportions. The solution of the Couette inverse problem based on the parabolic model without a plug flow is verified through comparisons with the results of mini-cone slump experiments. Further, a procedure to characterize the dynamic yield stress of cement mixes is proposed to obtain a more accurate estimate of the rheology of the cement paste.

2. Theoretical analysis

2.1 Selection of rheological testing scheme

The rheological behavior of fresh cement pastes is based on the original and ideal double plate model. As shown in **Fig. 2**, the simplest device designed for assessing the rheological properties consists of two parallel plates [43]. Assuming that these plates have a rectangular cross section, the contact area between each plate and the paste is A, distance between the plates is h, and relative velocity of the two plates under the action of force F is v_{max}. Accordingly, the shear stress τ and shear rate $\dot{\gamma}$ can be respectively calculated as

$$\tau = \frac{F}{A} \quad (1)$$

$$\dot{\gamma} = \frac{v_{max}}{h} = \frac{d\gamma}{dt} \quad (2)$$

However, designing a rheometer with this ideal shape is impractical. Several common rheometer test systems, including the coaxial cylinder test [44], parallel plate test [45], and conical plate test [46], have been designed accordingly. Among these, the coaxial cylinder system involves rotational measurements whereas the parallel and conical plate systems involve oscillatory measurements. The small-amplitude oscillatory shear is commonly used to test the viscoelasticity of pastes, and the applied shear rate varies with time in the form of a sinusoidal function [47]. However, as the shear rate of cement pastes generally increases linearly or logarithmically in most tests (**Fig. 3(a)**), the rheological parameters are usually measured using a rotational coaxial cylinder.

When using a coaxial cylinder system for rheological assessments, further details of the specific rheological scheme need to be determined. There are two common rheological schemes: (1) rotational velocity or shear rate increases or decreases continuously over time (**Fig. 3(a)**), and (2) rotational velocity or shear rate increases or decreases step-by-step over time (**Fig. 3(b)**). The first method is usually used for calculations of the thixotropic hysteresis loop area, and the second method is called the "multiple step method" because of its step-like appearance. Before analyzing the difference between these two rheological schemes, it must be ensured that the rheological model represents the rheological behavior of the fluid in a stable flowing state. Therefore, a proper rheological testing system should be established to ensure that the paste flows stably at different shear rates [22, 48].

Because cement pastes are thixotropic, their microstructure changes with an increase in the shear rate or rotational velocity. However, it takes time to destroy and rebuild this microstructure. Therefore, when the shear rate changes continuously, the paste cannot satisfy the basic conditions of a stable flow under a certain shear rate. If the shear rate cannot be kept constant for a period of time, the test shear stress may be higher or lower than the real shear stress, as shown in **Fig. 1**. Unfortunately, the steady-state approach provides information regarding only the asymptotic shear stress vs. shear rate or viscosity vs. shear rate relationships; it does not provide information about the dynamic thixotropic response. In this regard, the multiple step method can easily enable the paste to achieve a steady state in the broader context of time-dependent rheological behavior and thereby improve the accuracy of the test without considering the influence of thixotropic dynamics on the calculation of the rheological parameters. **Fig. 4** shows the variation of the torque with time, where N of each step remains constant within 10 s. **Fig. 4** shows that T fluctuates when N decreases from one step to the next. When T remains constant, the paste changes from an unsteady to a steady state, during which time the test data can be used to accurately calculate the rheological parameters of cement pastes.

A more important reason for not using the continuous change in the shear rate or the rotational velocity to directly test the rheological parameters of cement pastes is the Couette inverse problem [49]. The Couette inverse problem involves the transformation of the relationship between τ and $\dot{\gamma}$ based on different rheological models into the relationship between T and N measured using a rheometer. For a coaxial cylinder system, the relationship between τ and T and that between $\dot{\gamma}$ and $\omega(r)$ (angular velocity at radius r) are respectively given as [39, 43]

$$\tau = \frac{T}{2\pi h r^2} \tag{3}$$

$$\dot{\gamma} = r\frac{d\omega(r)}{dr} \tag{4}$$

where h is the height of the inner cylinder submerged in cement paste (m), and r is the radial coordinate (m).

Eqs. (3) and (4) show that although the conversion formulas of torque and shear stress are relatively simple, the shear rate and rotational velocity are linked with a differential relationship. The rheometer can only derive data pairs of rotational velocity and torque but not a continuous functional curve. Because continuity is a necessary condition for derivability, the shear rate and rotational velocity of the fresh cement paste cannot be directly transformed using Eq. (4). Therefore, the multiple step method was chosen to calculate the dynamic yield stress of fresh pastes in this study.

2.2 Limitations of normal rheological models

After determining the rheological scheme, the next step is to identify the rheological model to be used for characterizing the relationship between τ and $\dot{\gamma}$ of fresh cement pastes. The Bingham model is used most commonly to characterize cement mixes, which involve a combination of an ideal Newtonian fluid and a Saint-Venant ideal plastic solid [50]. In fresh cement mixes, assuming that no network structure exists between noncolloidal particles, the yield behavior mostly depends on the interaction between colloidal particles that results in the formation of a dense continuous network structure between them [2, 28]. This process makes the mix viscous owing to the cohesion and dynamic friction between particles that hinder the flow behavior; here, the viscosity reflects the deformation speed of the paste after destruction [40, 51]. The Bingham model is given by Eq. (5),

where τ_0 is the dynamic yield stress fitted using this model (Pa) and μ_p, a parameter unique to this model, is the plastic viscosity (Pa·s). When the Bingham model is assumed to be the constitutive equation of cement paste, the corresponding solution to the Couette inverse problem is obtained using the Reiner–Riwlin equation (Eqs. (6) and (7)) [52], where R_1 and R_2 are the inner and outer cylinder radius of the rheometer, respectively.

$$\tau = \tau_{0,B} + \mu_p \cdot \dot{\gamma}\,, \tau \geq \tau_0$$

$$\dot{\gamma} = 0\,, \tau < \tau_0 \tag{5}$$

$$\tau_{0,B} = \frac{G_B}{4\pi h}\left(\frac{1}{{R_1}^2} - \frac{1}{{R_2}^2}\right)\frac{1}{\ln\left(R_2/R_1\right)} \tag{6}$$

$$\mu = \frac{H_B}{8\pi^2 h}\left(\frac{1}{{R_1}^2} - \frac{1}{{R_2}^2}\right) \tag{7}$$

However, in the presence of different admixtures and environmental conditions, fresh cement pastes generally behave as a non-Newtonian fluid, thereby leading to errors in the calculation of rheological parameters when using the Bingham model as the constitutive equation. Therefore, the modified Bingham model (Eq. (8)) and H-B model (Eq. (9)) are frequently used to characterize the degree of deviation from the linear relationship between τ and $\dot{\gamma}$, where μ and c are the linear and quadratic terms of the modified Bingham model and K is the consistency factor of the H-B model.

$$\tau = \tau_{0,MB} + \mu\dot{\gamma} + c\dot{\gamma}^2 \tag{8}$$

$$\tau = \tau_{0,HB} + K\dot{\gamma}^n \tag{9}$$

Many models can describe the degree of shear thickening and thinning. In particular, the Lu Gang model [53], Vom Berg model [54], and Carreau model [55] can be used to describe the rheological behavior of non-Newtonian fluids. Nonetheless, the modified Bingham model and H-B model are still used most commonly to characterize the rheological behavior of non-Newtonian fluids owing

to their small number of unknown parameters and simple forms of equations.

Feys et al. [39] and Heirman et al. [40] proposed solutions for the Couette inverse problem based on the modified Bingham model and H-B model, respectively. However, Li et al. [41] found errors in the derivations of these solutions. They claimed that Heirman et al. [40] used an incorrect hypothesis, stating that the solution of the Couette inverse problem based on the H-B model and the expression of the H-B model should have the same exponential form. However, according to the relationship between the shear rate and the rotational velocity, their relationship is a differential function rather than an ordinary one; therefore, this hypothesis remains unproven. Further, the separation of r and ω in Eq. (14) as described by Feys et al. [39] is incomplete. The left-hand side of the equation is in the form $f(r)\mathrm{d}r$, whereas the right-hand side is in the form $g(r, \omega)\mathrm{d}\omega$; this leads to an error in the next equation. As an alternative, Li et al. [41] provided *N*-*T* equations based on different rheological models with the assumption that the functional relationship between τ and $\dot{\gamma}$ of the measured fluid can be characterized by Eq. (10). Substituting Eqs. (10) and (4) into Eq. (3) and moving the torque T to the left-hand side gives

$$\tau = f(\dot{\gamma}) \tag{10}$$

$$T = 2\pi h r^2 f(r\frac{d\omega}{dr}) \tag{11}$$

For the fluid investigated, with an increase in τ, $\dot{\gamma}$ will also increase, indicating that Eq. (10) is a monotonic increasing function with an inverse function f^{-1}. Solving f^{-1} and separating the values of r and ω gives

$$d\omega = \frac{1}{r} f^{-1}(\frac{T}{2\pi h r^2})\, dr \tag{12}$$

Integrating Eq. (12) gives Eq. (13), where Ω is the relative angular velocity between the outer and

the inner cylinders of the rheometer.

$$\int_0^{\Omega} d\omega = \int_{R_1}^{R_2} \frac{1}{r} f^{-1}\left(\frac{T}{2\pi h r^2}\right) dr \tag{13}$$

Further solving the original function and rearranging the terms in Eq. (13) gives

$$\begin{aligned} \Omega &= \int_{R_1}^{R_2} \frac{r^2}{r^3} f^{-1}\left(\frac{T}{2\pi h r^2}\right) dr \\ &= \int_{R_1}^{R_2} -\frac{r^2}{2} f^{-1}\left(\frac{T}{2\pi h r^2}\right) d\frac{1}{r^2} \\ &= -\frac{1}{2}\int_{R_1}^{R_2} \frac{2\pi h r^2}{M} f^{-1}\left(\frac{T}{2\pi h r^2}\right) d\frac{T}{2\pi h r^2} \end{aligned} \tag{14}$$

Substituting Eq. (3) into Eq. (14) and substituting the rotational velocity N for the angular velocity Ω gives

$$N = -\frac{1}{2}\int_{\tau_1}^{\tau_2} \frac{1}{\tau} f^{-1}(\tau) d\tau \tag{15}$$

Substituting Eq. (10) into Eq. (15) gives

$$N = -\frac{1}{2}\int_{\dot{\gamma}_1}^{\dot{\gamma}_2} \frac{\dot{\gamma} \cdot f'(\dot{\gamma})}{f(\dot{\gamma})} d\dot{\gamma} \tag{16}$$

Eqs. (15) and (16) can both be used to solve the Couette inverse problem of a coaxial cylinder rheometer. Specifically, Eq. (15) can be used to calculate the *N*-*T* relation when f^1 can be easily solved, and Eq. (16) can be chosen when f' can be conveniently obtained. Substituting the expressions of a Newtonian fluid model and the Bingham model into Eq. (15) gives two function expressions that are the same as the Margule [56] and Reiner–Riwlin equations. This verifies the accuracy of the derivation process.

Substituting Eqs. (15) and (16) with the expressions for the modified Bingham model and H-B model and simplifying the corresponding polynomials gives the *N*-*T* relations based on the modified Bingham model and H-B model as shown in Eqs. (17) and (18), respectively.

$$N = \frac{\mu}{2c}\ln\left(\frac{R_1}{R_2}\right) + \frac{1}{2c}\cdot\left(\sqrt{\mu^2 - 4c\tau_0 + 4c\frac{T}{2\pi h{R_1}^2}} - \sqrt{\mu^2 - 4c\tau_0 + 4c\frac{T}{2\pi h{R_2}^2}} + \sqrt{4c\tau_0 - \mu^2}\right.$$

$$\cdot arctan\sqrt{\frac{\mu^2 - 4c\tau_0 + 4c\frac{T}{2\pi h{R_1}^2}}{4c\tau_0 - \mu^2}} - \sqrt{4c\tau_0 - \mu^2}$$

$$\left.\cdot arctan\sqrt{\frac{\mu^2 - 4c\tau_0 + 4c\frac{T}{2\pi h{R_2}^2}}{4c\tau_0 - \mu^2}}\right) \tag{17}$$

$$N = -\frac{n}{2}(\dot{\gamma}_2 - \dot{\gamma}_1) + \frac{n}{2}\int_{\dot{\gamma}_1}^{\dot{\gamma}_2}\frac{1}{1 + \frac{\kappa}{\tau_0}\dot{\gamma}^n}d\dot{\gamma} \tag{18}$$

Eqs. (17) and (18) show that the *N*-*T* equation based on the H-B model does not have a solution for the latter part of the integral in the real number range. Although the form of the modified Bingham model itself is relatively simple, the solution of the Couette inverse problem as calculated using the modified Bingham model is very complex and cannot be used as a generalized formula. Therefore, a new rheological model whose form and expression for the solution of the Couette inverse problem solution are both relatively simple is needed.

2.3 Solution based on the Parabolic model

Although the rheological model and its solution for the Couette inverse problem should be as concise as possible, the model must be capable of characterizing at least the yield behavior and the nonlinear variation. Fresh cement paste can be regarded as a fluid that exhibits yield behavior. Before its internal structure is destroyed, an external force greater than its static yield stress is required to enable it to flow. At the same time, owing to the influence of admixtures, temperature, and time factors, τ-$\dot{\gamma}$ of most cement pastes does not show a simple linear relationship. In this light,

the rheological models and their solutions as presented by Li et al. [41, 57] were compared and screened. The Parabolic model and its *N*-*T* relationship function form were found to be relatively simple. Further, as with the modified Bingham model, the constant term of the Parabolic model could describe fluids with yield stress. A quadratic correction term was introduced to represent the degree of shear thickening or shear thinning. The expression of the Parabolic model and its solution for the dynamic yield stress are respectively given by

$$\dot{\gamma} = a + b\tau + c\tau^2 \tag{19}$$

$$\tau_{0,P} = \frac{-b + \sqrt{b^2 - 4ac}}{2c} \tag{20}$$

When $\dot{\gamma} = 0$, two solutions should exist for the one variable quadratic equation. However, because a rheological model has only one dynamic yield stress, when τ increases, $\dot{\gamma}$ increases accordingly. Therefore, a larger solution is taken as the value of the dynamic yield stress (Eq. (20)). Unlike in the modified Bingham model, the Parabolic model is a rheological model with the shear stress as an independent variable and the shear rate as a dependent variable [58]. Eq. (5) shows that the expressions for different value ranges of the Bingham model are determined by τ (e.g., for $\tau < \tau_0$, $\dot{\gamma} = 0$, and for $\tau \geq \tau_0$, $\tau = f(\dot{\gamma})$). Although the independent variable of the Bingham model is $\dot{\gamma}$, the piecewise expression of this model fully proves that the flow deformation is caused by the force.

Substituting Eq. (19) into Eq. (15) gives the following equation, where τ_1 and τ_2 are the shear stress of the measured fluid at the inner and the outer cylinders of the rheometer, respectively.

$$\begin{aligned} N &= -\frac{1}{2}\int_{\tau_1}^{\tau_2} \frac{1}{\tau}(a + b\tau + c\tau^2)d\tau \\ &= -\frac{1}{2}[aln\frac{\tau_2}{\tau_1} + b(\tau_2 - \tau_1) + \frac{1}{2}c({\tau_2}^2 - {\tau_1}^2)] \end{aligned} \tag{21}$$

The cylinder radii corresponding to τ_1 and τ_2 are R_1 and R_2, respectively. According to Eq. (3),

substituting the expressions of τ_1 and τ_2 into Eq. (21) gives the solution of the Couette inverse problem based on the Parabolic model.

$$N = a \cdot \ln\left(\frac{R_2}{R_1}\right) + \frac{b}{4\pi h}\left(\frac{1}{{R_1}^2} - \frac{1}{{R_2}^2}\right) \cdot T + \frac{c}{16\pi^2 h^2}\left(\frac{1}{{R_1}^4} - \frac{1}{{R_2}^4}\right) \cdot T^2 \tag{22}$$

2.4 Influence of plug flow

In a coaxial cylinder system, as the cylinder rotates, fresh cement pastes with different radii are subjected to different shear stress. Owing to the existence of the yield stress in cement pastes, when the shear stress at a certain radius is less than the dynamic yield stress, the shear rate at this radius is zero and no relative movement occurs between adjacent layers. This phenomenon is called plug flow (see **Fig. 5**) [39, 59, 60]. By moving τ of Eq. (3) to the right-hand side of the equation and R_p to the left-hand side of the equation, the radius of the plug flow can be calculated as [43]

$$R_p = \sqrt{\frac{T}{2\pi\tau_0 h}} \tag{23}$$

Wallevik et al. [43] provided an equation for calculating the shear rate of fluids at the inner cylinder wall based on the Bingham model by using a coaxial cylinder rheometer. However, according to Wallevik's equation, the shear rate depends on the plug radius, rheometer size, and rheological properties of the fluid. Because of its complex iterative calculation and the need to determine additional parameters, a more concise rheological test method is needed considering the influence of the plug flow.

2.5 Verification of calculation results

The accuracy of the dynamic yield stress calculated by the above process can be verified through numerical simulations (computational fluid dynamics) or macroscopic experimental results. A computer-based numerical simulation can be applied to cement-based materials to understand not only the computer technology but also the rheological characteristics of pastes. Considering that most cement pastes are non-Newtonian fluids, although a few numerical simulation studies on them have already been conducted, this approach still needs to be validated.

The mini-cone slump flow method can be used to further verify the accuracy of the dynamic yield stress. The slump flow is commonly used to test the fluidity of pastes, mortars, and concrete mixes. Although several studies have proposed a relationship between the yield stress and the slump flow [61-64], most were usually used to convert the concrete slump flow into the yield stress. The slump flow for cement pastes has much smaller diameters, making the prediction of the yield stress challenging [65]. By comprehensively considering the influence of surface tension, Roussel et al. [66] proposed the following relationship between the mini-cone slump flow diameter L and the yield stress $\tau_{0,R}$:

$$\tau_{0,R} = \frac{225\rho_{paste} g {V_{cone}}^2}{128\pi^2 (\frac{L}{2})^5} - \frac{0.005\left(\frac{L}{2}\right)^2}{V_{cone}} \quad (24)$$

Because the result of the mini-cone test indicates the final expansion diameter of the paste, when the combined stress of each microelement of the paste is lower than its own yield stress, the paste will no longer flow; this corresponds to the definition of dynamic yield stress. Although the mini-cone slump test is based on a semiempirical deduction, Roussel's equation remains widely used, thus somewhat verifying the effectiveness of this formula. Therefore, it is reasonable to consider $\tau_{0,R}$ calculated using Eq. (24) as the dynamic yield stress of pastes from a macroscopic view. Notably,

in this study, the mini-cone test is not only regarded as an accurate dynamic yield stress calculation method but also as the macroscopic reference result. By comparing these results with those obtained from different rheological tests and calculating their differences, the accuracy of the proposed method can be further verified.

3. Calculation example

3.1 Materials and methodology

Portland Cement (PC) Type 1 42.5 (China United Cement Corporation) that conformed to the GB 8076-2008 standard was used as the main binder. Class F fly ash (FA), ground granulated blast furnace slag (GGBS), limestone powder (LP), and viscosity modifying agent (VMA) obtained from Hunan Province were also incorporated in the prepared mixes. **Table 1** lists the chemical compositions of PC, FA, GGBS, and LP and the corresponding densities of all cementitious materials. VMA (China Shandong Highway New Material Technology Co. Ltd.) consists of silica fume (SF), LP, and hydroxypropyl methylcellulose (HPMC); it is an important thickening component used in high-speed railway ballastless track self-compacting concrete.

Fig. 6 shows the particle size distributions of PC, FA, GGBS, and LP as determined using an auto laser particle size analyzer (Jinan Runzhi Science and Technology Ltd.). To improve the fluidity of the prepared pastes and increase the dispersion of the cementitious particles, a polycarboxylate-based superplasticizer (PCE; Shanxi Jiawei New Material Co. Ltd.) with a 27% water-reducing rate and 33.1% solid content was prepared. **Table 2** lists the mixture proportions of the prepared mixes.

Thirteen mixtures were prepared, including one containing only PC as the reference group and 12 in which PC was partially replaced with FA, GGBS, LP, and VMA.

An Anton Paar MCR 102 rheometer was used to assess the rheology of these mixes in line with the requirements of ISO 3219 [67]. A CC27-type rotator with an effective height of 40 mm was used. Its inner and outer diameters were 26.661 and 28.913 mm, respectively. The external cylinder remained stationary during the test.

The mini-cone slump flow test of the fresh cement pastes was performed in line with their fluidity (Chinese Code GB/T8077-2012). The diameter of the upper and lower openings was respectively 36 and 60 mm, and the height was 60 mm. The cementitious materials were placed into the mixing pot and mixed evenly, following which water and PCE were added into the mixing pot. Mixing was performed at 60 rpm for 90 s, followed by a pause for 15 s, after which further mixing was performed at 120 rpm for 90 s. After sufficient mixing, the paste was injected into the mini-cone, which was then lifted vertically. When the paste was no longer flowing, the maximum diameter in different directions was measured. The test was repeated three times for each mix proportion. Because the shape of the paste after flowing was usually different from that of the standard circle (**Fig. 7**), the center of the base plate was taken as the center of the circle, and the average value of diameters L_1, L_2, L_3, and L_4 in four directions was taken as the final fluidity L, as shown in Eq. (25).

$$L = \frac{L_1 + L_2 + L_3 + L_4}{4} \tag{25}$$

3.2 Calculation process

The Reiner–Riwlin equation is currently used most often to calculate the yield stress of fresh cement-based materials. However, because the shear stress and shear rate of most cement-based materials do not have a simple linear relationship, the calculation method using the Bingham model as the constitutive equation will inevitably have errors. Simultaneously, the existence of the plug flow cannot be ignored. When the torque of the rheometer rotator is too small, the minimum shear stress (τ_{min}) corresponding to the maximum radius (i.e., the inner wall of the outer cylinder) is lower than the yield stress calculated using the test points. At this time, a certain plug flow area will exist near the outer cylinder, and the fluid between the inner and the outer cylinders will not flow as shown for the parallel plate model in **Fig. 2**. Therefore, the solution of the Couette inverse problem based on the Parabolic model was used to calculate the dynamic yield stress under the condition of excluding the error points caused by the plug flow. The specific calculation steps were as follows:

(1) The solution of the Couette inverse problem based on the Parabolic model was used to fit all *N*-*T* data pairs of each paste, and three parameters *a*, *b*, and *c* in the Parabolic model were obtained.

(2) The values of *a*, *b*, and *c* were substituted into Eq. (20), and the dynamic yield stress was calculated without considering the influence of the plug flow.

(3) According to Eq. (3), τ_{min} corresponding to the minimum torque in the coaxial cylinder was calculated to show its relationship with the dynamic yield stress. When τ_{min} was lower than the

dynamic yield stress, a plug flow occurred in the paste. The test points with minimum torque were deleted, and the remaining test points were fit and recalculated according to the above steps. The calculation cannot be stopped until the minimum shear stress is greater than the dynamic yield stress. Finally, the calculated value obtained after excluding the influence of plug flow gave the real dynamic yield stress.

Fig. 8 shows all test points numbered according to the order of torque from small to large, where each test point corresponds to a *N*-*T* data pair. **Fig. 9** shows the rheological scheme applied in this study. The scheme was divided into three phases. First, the rotator velocity was linearly increased to the maximum value and then kept constant for 60 s to create a steady-state shear test environment before the rheological test so as to ensure that the shear state of each paste was consistent; this was also referred to as the pre-shearing process. Then, the velocity was gradually decreased in steps lasting 10 s, followed by a drop to the next step within 5 s. The whole test process lasted for 360 s.

3.3 Results

Fig. 10 shows the *N*-*T* curves of the pastes after incorporating different admixtures, and **Fig. 11** shows the test results for fluidity. A comparison of the *N*-*T* curves of different pastes showed that the torque of pastes incorporating FA and GGBS at the same rotational velocity reduced when compared with that of pure cement paste, and VMA increased the torque at each test point. When GGBS and VMA were added, the *N*-*T* curve gradually deviated from linear growth, indicating the shear thickening of the paste. The larger the GGBS and VMA contents, the higher was the shear

thickening degree. At this point, a large error could occur in the results if the Bingham model was used as the constitutive equation. The deviation of the *N*-*T* curve of cement paste from the linear relationship illustrates the importance of using other models as constitutive equations. The addition of FA and GGBS gradually increased the fluidity of the pastes, whereas LP did not affect the fluidity and VMA decreased the fluidity to a certain extent.

The 16 test points of each paste, shown in **Fig. 10**, were fitted in the form of a quadratic function to obtain the constant term and the coefficients of the primary and quadratic terms, which correspond to $a \cdot \ln(\frac{R_2}{R_1})$, $\frac{b}{4\pi h}\left(\frac{1}{R_1^2}-\frac{1}{R_2^2}\right)$, and $\frac{c}{16\pi^2 h^2}\left(\frac{1}{R_1^4}-\frac{1}{R_2^4}\right)$ in Eq. (22), respectively. This was followed by the calculation of the parameters *a*, *b*, and *c* in the Parabolic model. The yield stress without considering the plug flow was obtained using Eq. (20). Then, the minimum shear stress was calculated using Eq. (3). If the minimum shear stress was lower than the calculated yield stress, it indicates the occurrence of a plug flow in the paste during the test. In this case, point 1 with the minimum torque was deleted and the above calculation process was repeated for the remaining 15 test points until the minimum shear stress was larger than the yield stress [57].

Table 3 shows the results of the assessment of the presence of a plug flow in the rheological test of 13 groups. The differences in the number of test points removed by considering the influence of a plug flow for pastes under different mix proportions could be observed. For pure cement pastes and pastes incorporating only FA, no plug flow occurred in the whole test process, thereby eliminating the need to remove any test points. However, one test point for three groups of pastes mixed with GGBS; two test points for pastes with 5 wt% LP; and one test point for pastes incorporating 10 wt%

LP, 5 wt% VMA, and 10 wt% VMA needed to be removed. Overall, composite pastes with high yield stresses usually involved the removal of 1–2 test points. Considering the size of the inner and outer coaxial cylinders, the limited gap distance was associated with the effort to avoid a plug flow during the test. Nonetheless, a plug flow still occurred in the pastes, indicating the necessity to eliminate the error points when the torque is too small during the test process.

Fig. 12 illustrates a comparison between the calculation results obtained using the Reiner–Riwlin model, the Parabolic model without and with the consideration of the influence of a plug flow, and based on fluidity. To evaluate the results, the deviation *D* was defined as the sum of the squares of the difference of the yield stress obtained using the two calculation methods for the abscissa and ordinate in **Fig. 12**. A comparison of **Fig. 12(a)–(c)** revealed that the yield stress calculated using the Reiner–Riwlin equation was quite different from that calculated based on the fluidity, and the test points were too discrete to use an appropriate function to characterize their relationship. Compared with the calculation results based on the Reiner–Riwlin equation, those based on the Parabolic model without considering the plug flow were very close to the results obtained based on fluidity. After removing the erroneous *N*-*T* test points, the *D* value reached a minimum, indicating that the two yield stress values became closer than they did in the absence of the plug flow. Although the calculation results of the dynamic yield stress based on fluidity were not extremely accurate, the above results showed that the proposed calculation method based on the Parabolic model in consideration of the plug flow was reasonable and provided adequate precision.

4. Conclusion

This study aimed to identify and propose an accurate method for calculating the dynamic yield stress of fresh cement pastes, during which the influence of the plug flow and shear thickening or shear thinning were eliminated. Owing to the existence of thixotropy, it takes time to destroy and rebuild the microstructure in cement pastes. Therefore, compared with the method of continuously increasing or decreasing the rotational velocity, the multiple step method was found to be more suitable for assessing the rheological properties of cement pastes in the steady state. In a coaxial cylinder test system, the Couette inverse problem presents unavoidable challenges. Generally, the simple Bingham model is not used as the constitutive equation of fresh cement paste. However, the solution of the Couette inverse problem based on the modified Bingham model and the H-B model is too complex or has no real number solution. An assessment of various rheological models suggested that the Parabolic model could serve as a convenient method for calculating the dynamic yield stress of cement pastes. When the rheometer rotator velocity was low, a plug flow could occur on the inner wall of the outer cylinder, necessitating the exclusion of several test points when the minimum shear stress was less than the calculated dynamic yield stress. This method of calculating the dynamic yield stress was also verified through comparisons with the results obtained using mini-cone slump flow tests, and it indicated the accuracy of this theoretical analysis.

Acknowledgments

This work was financially supported by the National Natural Science Foundation of China (grant

nos. 51678568 and 51678569), China Railway 21st Bureau Group Science and Technology Plan Project (20180A), and China Scholarship Council.

References

[1] Toutou Z, Roussel N. Multi scale experimental study of concrete rheology: from water scale to gravel scale. Mater Struct. 2006;39(2):189-199. https://doi.org/10.1617/s11527-005-9047-y

[2] Perrot A, Lecompte T, Khelifi H, Brumaud C, Hot J, Roussel N. Yield stress and bleeding of fresh cement pastes. Cem Concr Res. 2012;42(7):937-944. https://doi.org/10.1016/j.cemconres.2012.03.015

[3] Lowke D, Gehlen C. The zeta potential of cement and additions in cementitious suspensions with high solid fraction. Cem Concr Res. 2017;95:195-204. https://doi.org/10.1016/j.cemconres.2017.02.016

[4] Yahia A. Shear-thickening behavior of high-performance cement grouts-Influencing mix-design parameters. Cem Concr Res. 2011;41(3):230-235. https://doi.org/10.1016/j.cemconres.2010.11.004

[5] Liu Y, Shi CJ, Jiao DW, An XP. Rheological Properties, Models and Measurements for Fresh Cementitious Materials—A Short Review. J Chin Ceram Soc. 2017;45:708-716. (in Chinese) https://doi.org/10.14062/j.issn.0454-5648.2017.05.17

[6] Cheng HY, Wu SC, Li H, Zhang XQ. Influence of time and temperature on rheology and flow performance of cemented paste backfill. Constr Build Mater. 2020;231:117117. https://doi.org/10.1016/j.conbuildmat.2019.117117

[7] Li ZG, Cao GD. Rheological behaviors and model of fresh concrete in vibrated state, Cem

Concr Res. 2019;120:217-226. https://doi.org/10.1016/j.cemconres.2019.03.020

[8] Yang H, Lu CR, Mei GX. Shear-Thickening Behavior of Cement Pastes under Combined Effects of Mineral Admixture and Time. J Mater Civ Eng. 2018;30(2):04017282. https://doi.org/10.1061/(ASCE)MT.1943-5533.0002123

[9] Ke GJ, Zhang J, Xie SX, Pei TC. Rheological behavior of calcium sulfoaluminate cement paste with supplementary cementitious materials. Constr Build Mater. 2020;243:118234. https://doi.org/10.1016/j.conbuildmat.2020.118234

[10] Ma KL, Feng J, Long GC, Xie YJ. Effects of mineral admixtures on shear thickening of cement paste. Constr Build Mater. 2016;126:609-616. https://doi.org/10.1016/j.conbuildmat.2016.09.075

[11] Jiao DW, Shi CJ, Yuan Q. Influences of shear-mixing rate and fly ash on rheological behavior of cement pastes under continuous mixing. Constr Build Mater. 2018;188:170-177. https://doi.org/10.1016/j.conbuildmat.2018.08.091

[12] Xue ZL, Gan DQ, Zhang YZ, Liu ZY. Rheological behavior of ultrafine-tailings cemented paste backfill in high-temperature mining conditions. Constr Build Mater. 2020;253:119212. https://doi.org/10.1016/j.conbuildmat.2020.119212

[13] Güneyisi E, Gesoglu M, Naji N, İpek S. Evaluation of the rheological behavior of fresh self-compacting rubberized concrete by using the Herschel-Bulkley and modified Bingham models. Arch Civ Mech Eng. 2016;16(1):9-19. https://doi.org/10.1016/j.acme.2015.09.003

[14] Feys D, Verhoeven R, De Schutter G. Evaluation of time independent rheological models applicable to fresh self-compacting concrete. Appl Rheol. 2007;17(5):56244-1. https://doi.org/10.1515/arh-2007-0018

[15] Ahari RS, Erdem TK, Ramyar K. Time-dependent rheological characteristics of self-consolidating concrete containing various mineral admixtures. Constr Build Mater. 2015;88:134-142. https://doi.org/10.1016/j.conbuildmat.2015.04.015

[16] Aiad I. Influence of time addition of superplasticizers on the rheological properties of fresh cement pastes. Cem Concr Res. 2003;33(8):1229-1234. https://doi.org/10.1016/S0008-8846(03)00037-1

[17] Zhang QQ, Liu JZ, Liu JP, Han FY, Lin W. Effect of superplasticizers on apparent viscosity of cement-based material with a low water–binder ratio. J Mater Civ Eng. 2016;28 (9):04016085. https://doi.org/10.1061/(ASCE)MT.1943-5533.0001590

[18] Qian Y, Kawashima S. Distinguishing dynamic and static yield stress of fresh cement mortars through thixotropy, Cem. Concr. Compos. 86 (2018) 288-296. https://doi.org/10.1016/j.cemconcomp.2017.11.019

[19] Rubio-Hernández FJ, Adarve-Castro A, Velázquez-Navarro JF, Páez-Flor NM, Delgado-García R. Influence of water/cement ratio, and type and concentration of chemical additives on the static and dynamic yield stresses of Portland cement paste. Constr Build Mater. 2020;235:117744. https://doi.org/10.1016/j.conbuildmat.2019.117744

[20] Choi BI, Kim JH, Shin TY. Rheological model selection and a general model for evaluating the viscosity and microstructure of a highly-concentrated cement suspension. Cem Concr Res. 2019;123:105775. https://doi.org/10.1016/j.cemconres.2019.05.020

[21] Roussel N, Ovarlez G, Garrault S, Brumaud C. The origins of thixotropy of fresh cement pastes. Cem Concr Res. 2012;42(1):148-157. https://doi.org/10.1016/j.cemconres.2011.09.004

[22] Roussel N, Lemaître A, Flatt RJ, Coussot P. Steady state flow of cement suspensions: A

micromechanical state of the art. Cem Concr Res. 2010;40(1):77-84. https://doi.org/10.1016/j.cemconres.2009.08.026

[23] Roussel N, Bessaies-Bey H, Kawashima S, Marchon D, Vasilic K, Wolfs R. Recent advances on yield stress and elasticity of fresh cement-based materials. Cem Concr Res. 2019;124:105798. https://doi.org/10.1016/j.cemconres.2019.105798

[24] Chen MX, Li LB, Wang JA, Huang YB, Wang SD, Zhao PQ, et al. Rheological parameters and building time of 3D printing sulphoaluminate cement paste modified by retarder and diatomite. Constr Build Mater. 2020;234:117391. https://doi.org/10.1016/j.conbuildmat.2019.117391

[25] Ye H, Gao X, Zhang L. Influence of time-dependent rheological properties on distinct-layer casting of self-compacting concrete. Constr Build Mater. 2019;199:214-224. https://doi.org/10.1016/j.conbuildmat.2018.12.025

[26] Chen MX, Yang L, Zheng Y, Huang YB, Li LB, Zhao PQ, et al. Yield stress and thixotropy control of 3D-printed calcium sulfoaluminate cement composites with metakaolin related to structural build-up. Constr Build Mater. 2020;252:119090. https://doi.org/10.1016/j.conbuildmat.2020.119090

[27] Roussel N. A thixotropy model for fresh fluid concretes: theory, validation and applications. Cem Concr Res. 2006;36(10):1797-1806. https://doi.org/10.1016/j.cemconres.2006.05.025

[28] Mahaut F, Mokeddem S, Chateau X, Roussel N, Ovarlez G. Effect of coarse particle volume fraction on the yield stress and thixotropy of cementitious materials. Cem Concr Res. 2008;38(11):1276-1285. https://doi.org/10.1016/j.cemconres.2008.06.001

[29] Conte T, Chaouche M. Parallel superposition rheology of cement pastes. Cem Concr Compos. 2019;104. https://doi.org/10.1016/j.cemconcomp.2019.103393

[30] Tuyan M, Ahari RS, Erdem TK, Çakır ÖA, Ramyar K. Influence of thixotropy determined by different test methods on formwork pressure of self-consolidating concrete. Constr Build Mater. 2018;173:189-200. https://doi.org/10.1016/j.conbuildmat.2018.04.046

[31] Assaad J, Khayat K, Mesbah H. Assessment of thixotropy of flowable and self-consolidating concrete. ACI Mater J. 2003;100(2):99–107.

[32] Yuan Q, Zhou DJ, Li BY, Huang H, Shi CJ. Effect of mineral admixtures on the structural build-up of cement paste. Constr Build Mater. 2018;160:117-126. https://doi.org/10.1016/j.conbuildmat.2017.11.050

[33] Kolawole JT, Combrinck R, Boshoff WP. Rheo-viscoelastic behaviour of fresh cement-based materials: Cement paste, mortar and concrete. Constr Build Mater. 2020;248. https://doi.org/10.1016/j.conbuildmat.2020.118667

[34] Eom Y, Kim F, Yang SE, Son JS, Chae HG. Rheological design of 3D printable all-inorganic inks using BiSbTe-based thermoelectric materials. J Rheol. 2019;63(2):291-304. https://doi.org/10.1122/1.5058078

[35] Lafforgue O, Seyssiecq I, Poncet S, Favier J. Rheological properties of synthetic mucus for airway clearance. J Biomed Mater Res Part A. 2018;106(2):386-396. https://doi.org/10.1002/jbm.a.36251

[36] Kaleta-Jurowska A, Grzeszczyk S, Dziubiński M. Application of multiple step change in shear rate model for determination of thixotropic behaviour of cement pastes. J. Build. Eng. 2020;32:101494. https://doi.org/10.1016/j.jobe.2020.101494

[37] Ancey C. Solving the Couette inverse problem using a wavelet-vaguelette decomposition. J Rheol. 2005;49(2):441-460. https://doi.org/10.1122/1.1849181

[38] Yeow YL, Ko WC, Tang PP. Solving the inverse problem of Couette viscometry by Tikhonov regularization. J Rheol. 2000;44 (6):1335-1351. https://doi.org/10.1122/1.1308520

[39] Feys D, Wallevik JE, Yahia A, Khayat KH, Wallevik OH. Extension of the Reiner–Riwlin equation to determine modified Bingham parameters measured in coaxial cylinders rheometers. Mater Struct. 2013;46 (1-2):289-311. https://doi.org/10.1617/s11527-012-9902-6

[40] Heirman G, Vandewalle L, Van Gemert D, Wallevik O. Integration approach of the Couette inverse problem of powder type self-compacting concrete in a wide-gap concentric cylinder rheometer. J Non-Newton Fluid Mech. 2008;150(2-3):93-103. https://doi.org/10.1016/j.jnnfm.2007.10.003

[41] Li MY, Han JG, Liu Y, Yan PY. Integration approach to solve the Couette inverse problem based on nonlinear rheological models in a coaxial cylinder rheometer. J Rheol. 2019;63(1):55-62. https://doi.org/10.1122/1.5049565

[42] Joye DD. Shear rate and viscosity corrections for a Casson fluid in cylindrical (Couette) geometries. J Colloid Interface Sci. 2003;267(1):204-210. https://doi.org/10.1016/j.jcis.2003.07.035

[43] Wallevik OH, Feys D, Wallevik JE, Khayat KH. Avoiding inaccurate interpretations of rheological measurements for cement-based materials. Cem Concr Res. 2015;78:100-109. https://doi.org/10.1016/j.cemconres.2015.05.003

[44] Wallevik JE. Minimizing end-effects in the coaxial cylinders viscometer: Viscoplastic flow inside the ConTec BML Viscometer 3. J Non-Newton Fluid Mech. 2008;155(3):116-123.

https://doi.org/10.1016/j.jnnfm.2008.05.006

[45] Ozyurt N, Mason TO, Shah SP. Correlation of fiber dispersion, rheology and mechanical performance of FRCs. Cem Concr Compos. 2007;29(2):70-79. https://doi.org/10.1016/j.cemconcomp.2006.08.006

[46] Waffle L, Godin L, Harris LB, Kontopoulou M. Rheological and physical characteristics of crustal-scaled materials for centrifuge analogue modelling. J Struct Geol. 2016;86:181-199. https://doi.org/10.1016/j.jsg.2016.02.014

[47] Huang TJ, Yuan Q, Zuo SH, Shi CJ. Evolution of elastic behavior of alite paste at early hydration stages. J Am. Ceram. Soc. 2020;103(11):6490-6504. https://doi.org/10.1111/jace.17354

[48] Roussel N. Steady and transient flow behaviour of fresh cement pastes. Cem Concr Res. 2005;35(9):1656-1664. https://doi.org/10.1016/j.cemconres.2004.08.001

[49] Heirman G, Hendrickx R, Vandewalle L, Van Gemert D, Feys D, De Schutter G. et al. Integration approach of the Couette inverse problem of powder type self-compacting concrete in a wide-gap concentric cylinder rheometer: Part II. Influence of mineral additions and chemical admixtures on the shear thickening flow behaviour. Cem Concr Res. 2009;39(3):171-181. https://doi.org/10.1016/j.cemconres.2008.12.006

[50] Jeong J, Chuta E, Ramézani H, Guillot S. Rheological properties for fresh cement paste from colloidal suspension to the three-element Kelvin–Voigt model. Rheol Acta. 2020;59(1):47-61. https://doi.org/10.1007/s00397-019-01171-x

[51] Bentz DP, Ferraris CF, Galler MA, Hansen AS. Influence of particle size distributions on yield stress and viscosity of cement-fly ash pastes. Cem Concr Res. 2012;42(2):404-409. https://doi.org/10.1016/j.cemconres.2011.11.006

[52] Reiner M. Deformation and flow: an elementary introduction to theoretical rheology, HK Lewis. 1949. https://doi.org/10.1016/0095-8522(50)90067-5

[53] Lu G, Wang K, Rudolphi TJ. Modeling rheological behavior of highly flowable mortar using concepts of particle and fluid mechanics. Cem Concr Compos. 2008;30(1):1-12. https://doi.org/10.1016/j.cemconcomp.2007.06.002

[54] Vom Berg W. Influence of specific surface and concentration of solids upon the flow behaviour of cement pastes. Mag Concr Res. 1980;31(109):211-216. https://doi.org/10.1680/macr.1980.32.113.241

[55] Perrin CL, Tardy PM, Sorbie KS, Crawshaw JC. Experimental and modeling study of Newtonian and non-Newtonian fluid flow in pore network micromodels. J Colloid Interface Sci. 2006;295(2):542-550. https://doi.org/10.1016/j.jcis.2005.09.012

[56] Brabazon D, Browne DJ, Carr AJ. Experimental investigation of the transient and steady state rheological behaviour of Al–Si alloys in the mushy state. Mater Sci Eng. A-Struct Mater Prop Microstruct Process. 2003;356(1-2):69-80. https://doi.org/10.1016/S0921-5093(03)00158-8

[57] Li MY. Nonlinear rheological modeling of fresh cementitious materials. Tsinghua University 2018. (Doctoral dissertation) (in Chinese) https://doi.org/10.27266/d.cnki.gqhau.2018.000797

[58] Atzeni C, Massidda L, Sanna U, Comparison between rheological models for portland cement pastes. Cem Concr Res. 1985;15 (3):511-519. https://doi.org/10.1016/0008-8846(85)90125-5

[59] Wallevik JE. Rheology of particle suspensions: fresh concrete, mortar and cement paste with various types of lignosulfonates. Fakultet for ingeniørvitenskap og teknologi. 2003.

[60] Li MY, Liu Y, Han JG, Yan PY. Calculation of Rheological parameters of Cement-Based Materials Based on Solution to the Couette Inverse Problem. J Chin Ceram Soc. 2020;48(8):1-8.

(in Chinese) https://doi.org/10.14062/j.issn.0454-5648.20190748

[61] Ferraris CF, de Larrard F. Testing and modeling of fresh concrete rheology. 1998.

[62] Tregger N, Gregori A, Ferrara L, Shah S. Correlating dynamic segregation of self-consolidating concrete to the slump-flow test. Constr Build Mater. 2012;28(1):499-505. https://doi.org/10.1016/j.conbuildmat.2011.08.052

[63] Hu C, de Larrard F, Sedran T, Boulay C, Bosc F, Deflorenne F. Validation of BTRHEOM, the new rheometer for soft-to-fluid concrete. Mater Struct. 1996;29(10):620-631. https://doi.org/10.1007/BF02485970

[64] Wallevik JE. Relationship between the Bingham parameters and slump. Cem Concr Res. 2006;36(7):1214-1221. https://doi.org/10.1016/j.cemconres.2006.03.001

[65] Roussel N. Rheology of fresh concrete: from measurements to predictions of casting processes. Mater. Struct. 2007;40(10):1001-1012. https://doi.org/10.1617/s11527-007-9313-2

[66] Roussel N, Stéfani C, Leroy R. From mini-cone test to Abrams cone test: measurement of cement-based materials yield stress using slump tests. Cem Concr Res. 2005;35(5):817-822. https://doi.org/10.1016/j.cemconres.2004.07.032

[67] Postoy VV, Kukhtenko HP, Vyshnevska LI, Gladukh YV, Semchenko KV. Study of rheological behaviour of hydroxyethyl cellulose gels in the development of the composition and technology of the medicine with anti-inflammatory activity. Pharmacia. 2019;66(4):187-192. https://doi.org/10.3897/pharmacia.66.e37267

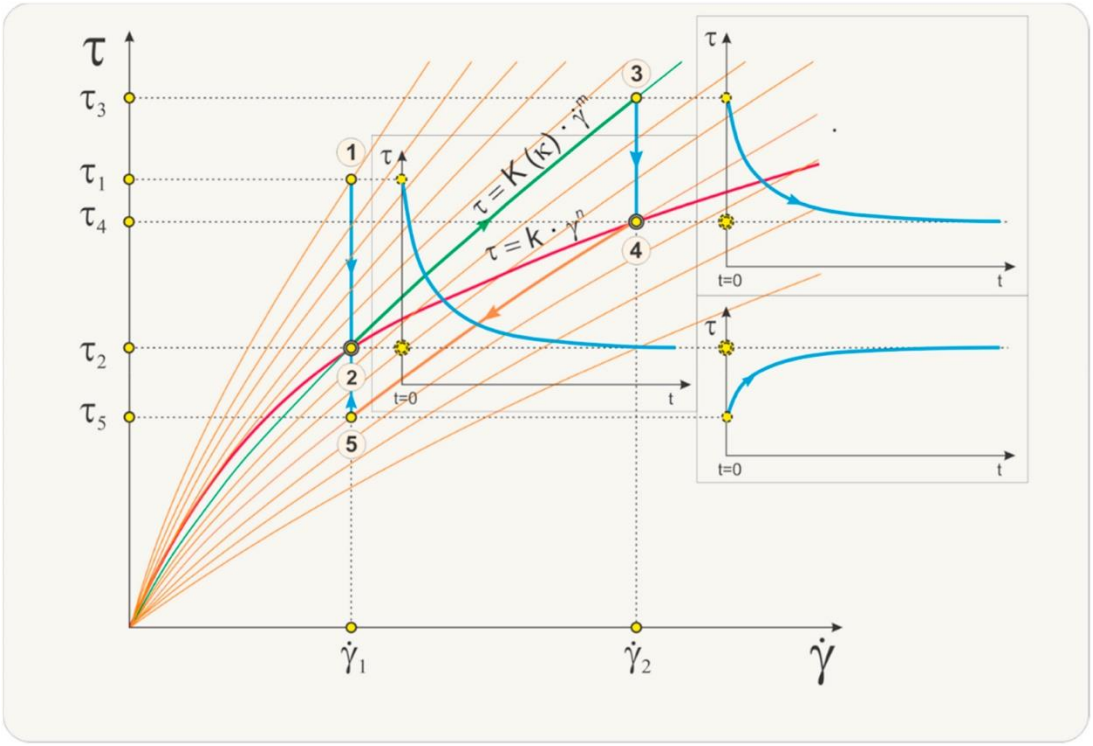

Fig. 1 Variation of shear stress with time for thixotropic fluid at different shear rates [36]

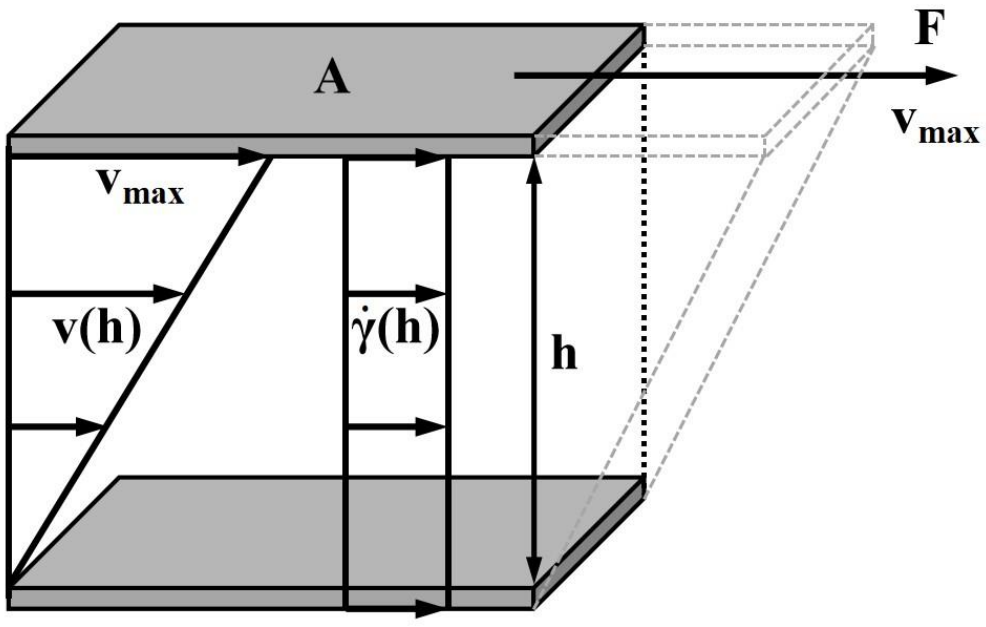

Fig. 2 Double parallel plate model for calculating rheological parameters of cement pastes

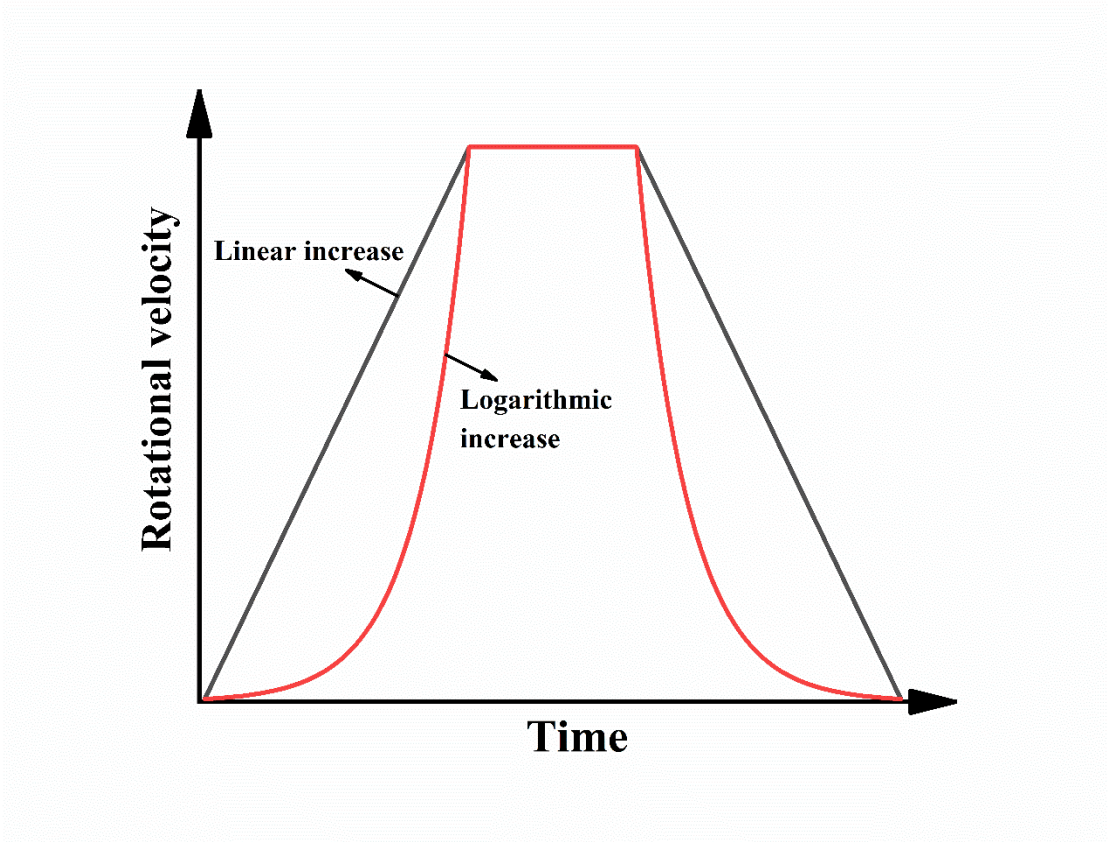

(a)

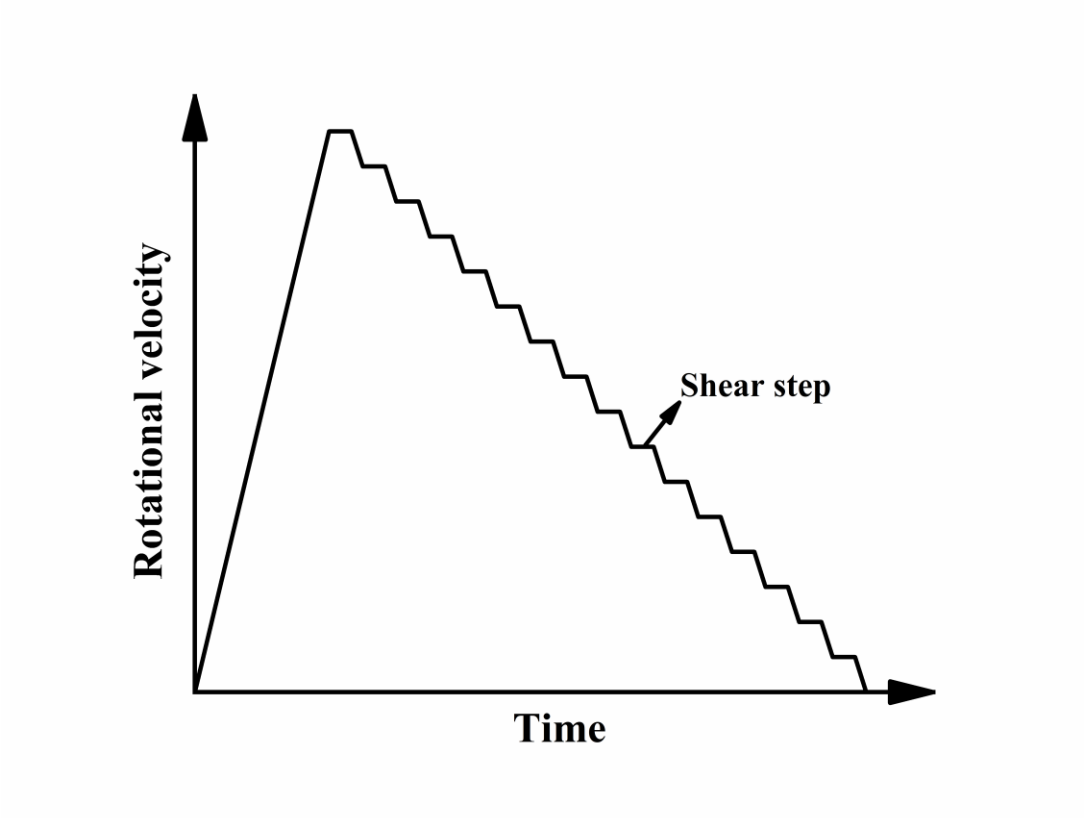

(b)

Fig. 3 Two different rheological schemes without pre-shear, showing (a) thixotropic hysteresis

loop method and (b) multiple step method

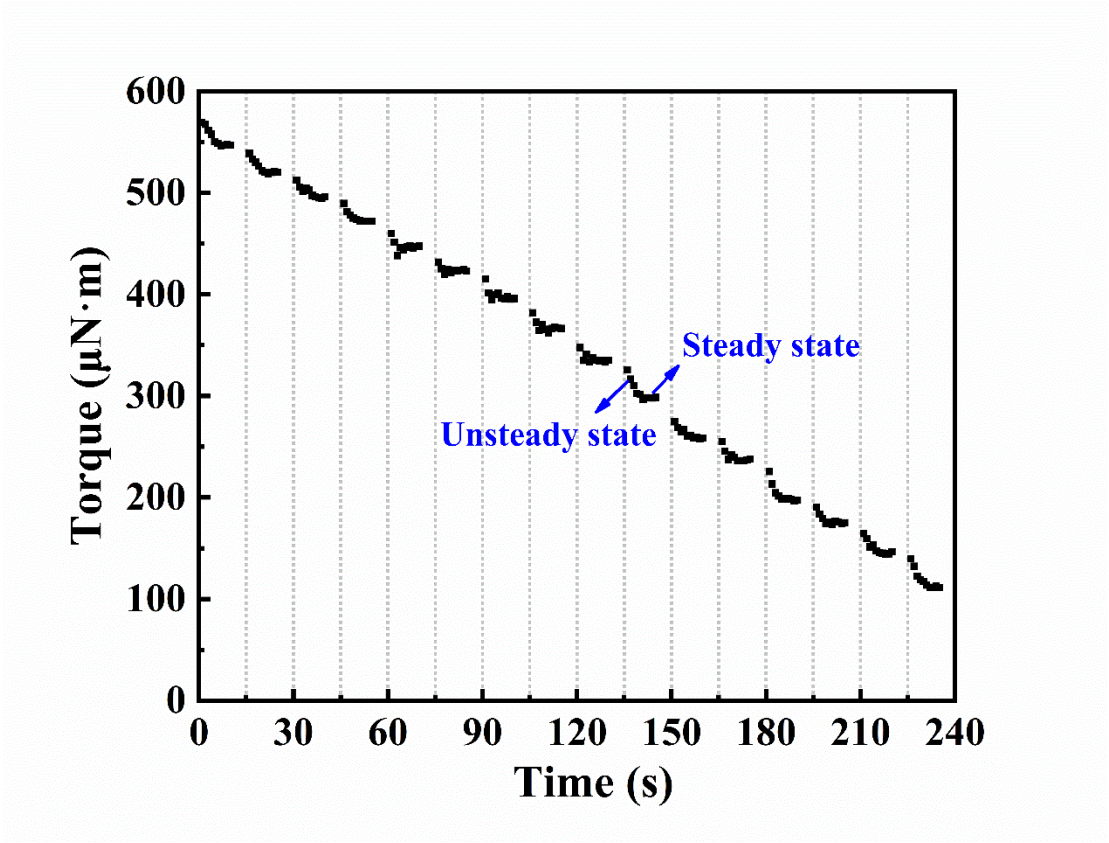

Fig. 4 Torque *vs.* time

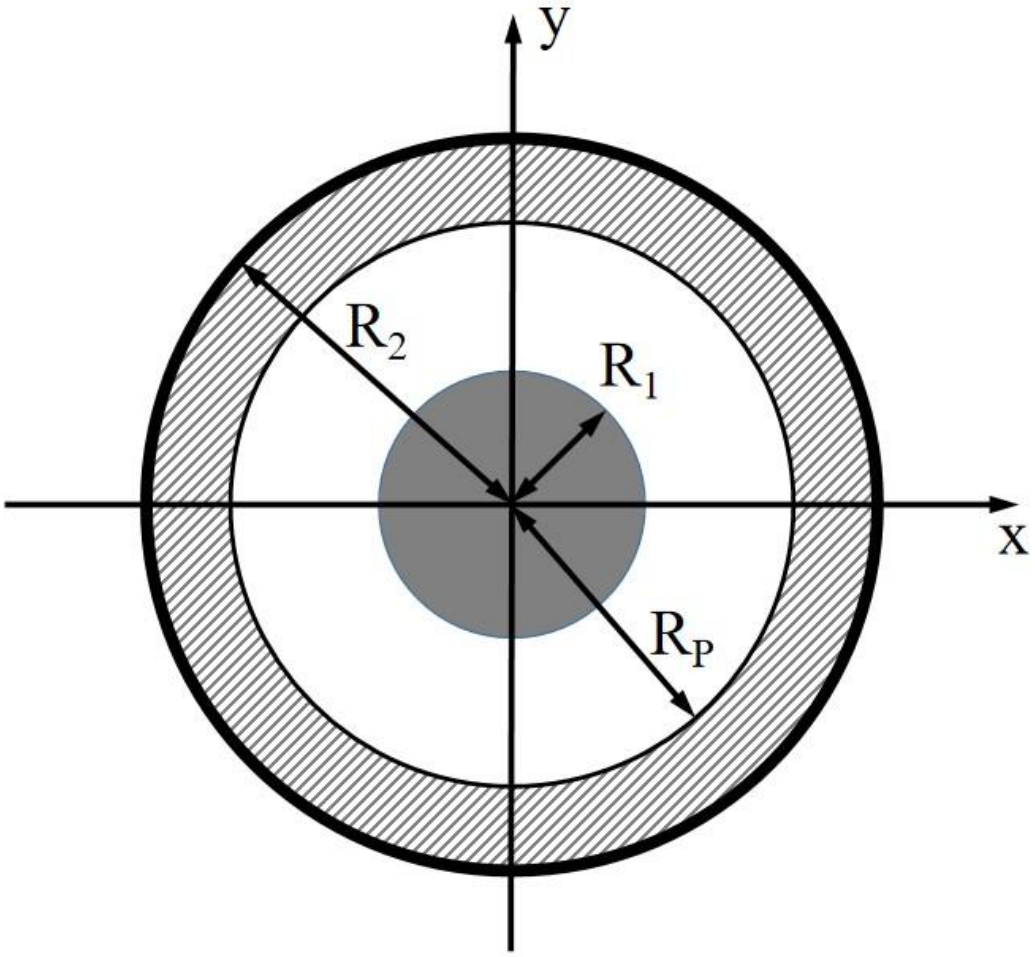

Fig. 5 Plug flow in coaxial cylinder system (R_1 = inner cylinder radius, R_2 = outer cylinder radius, R_p = plug flow radius)

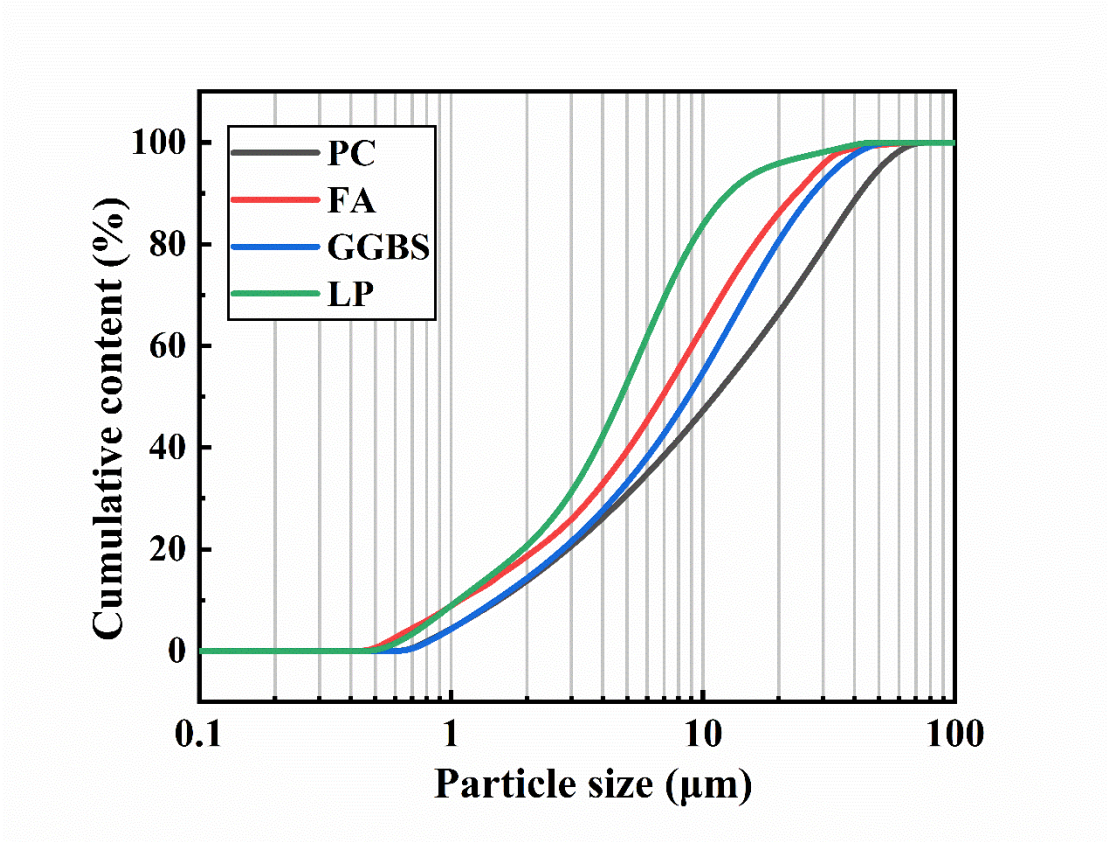

Fig. 6 Particle size distribution of cementitious materials

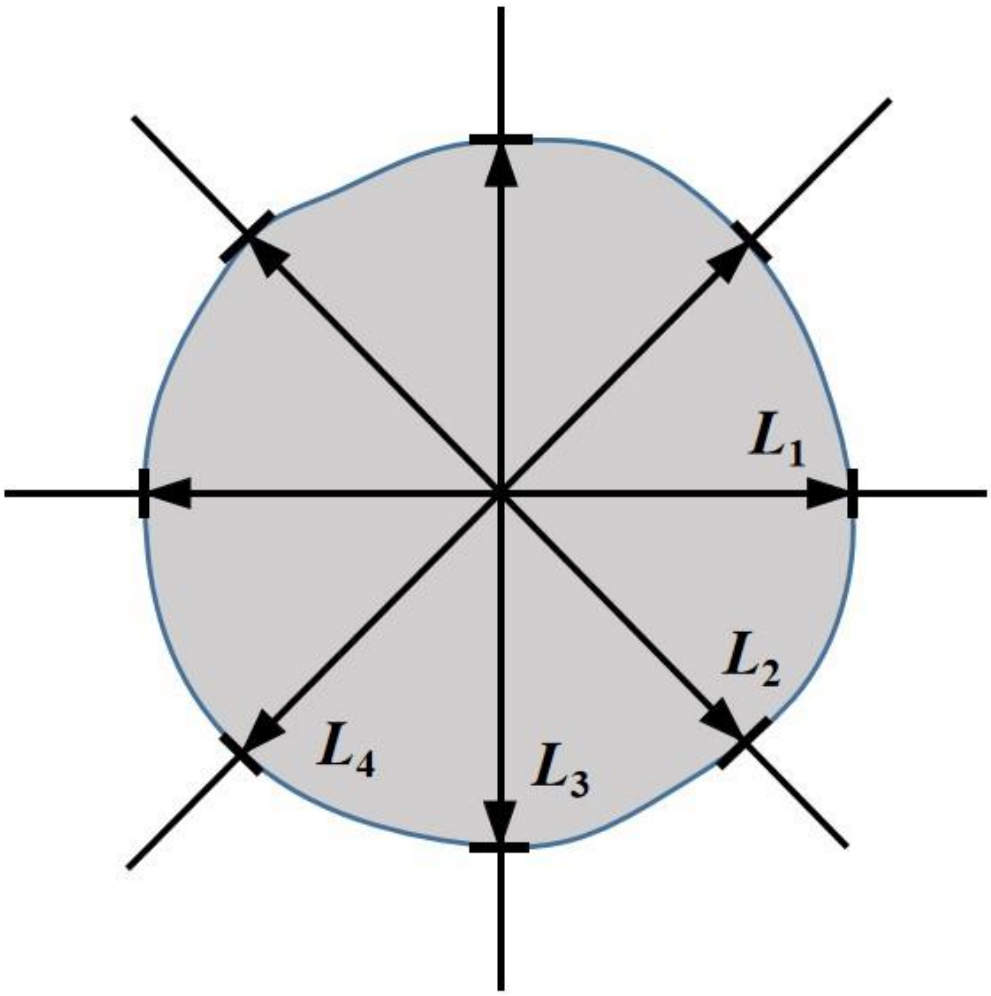

Fig. 7 Mini-cone slump flow test

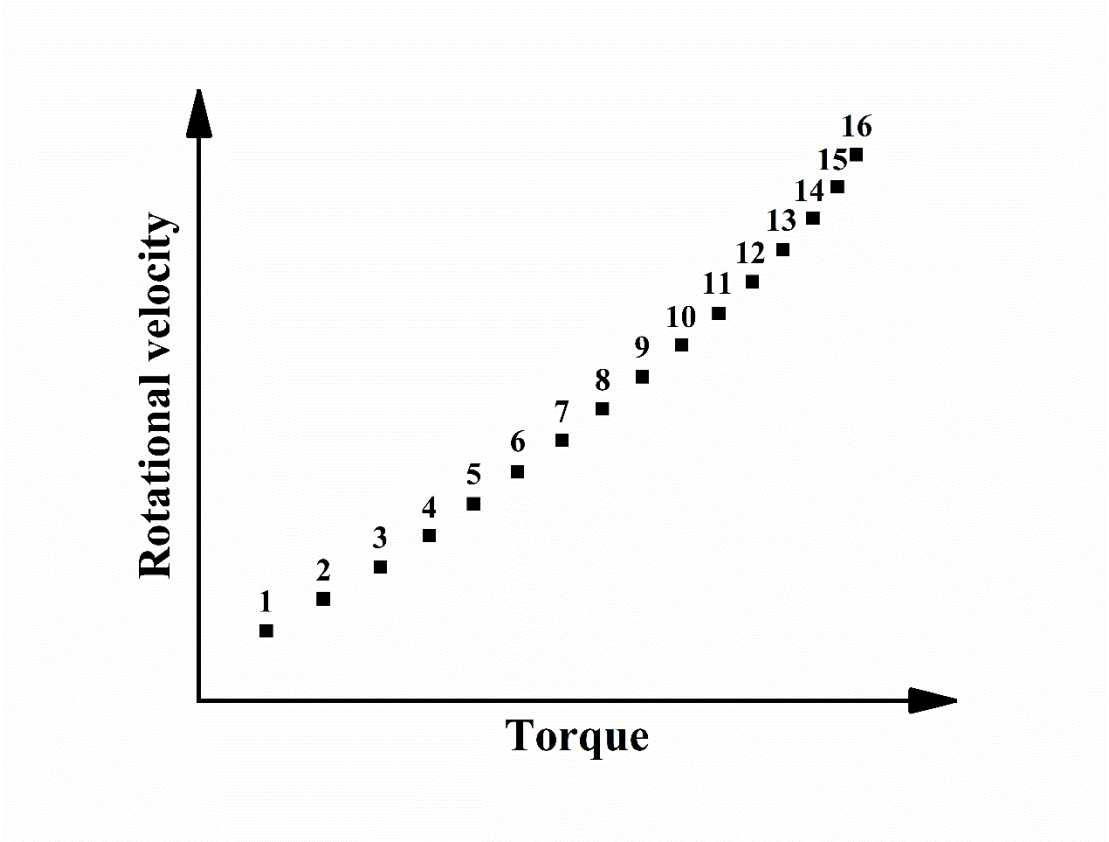

Fig. 8 Data points and number of paste used to calculate dynamic yield stress

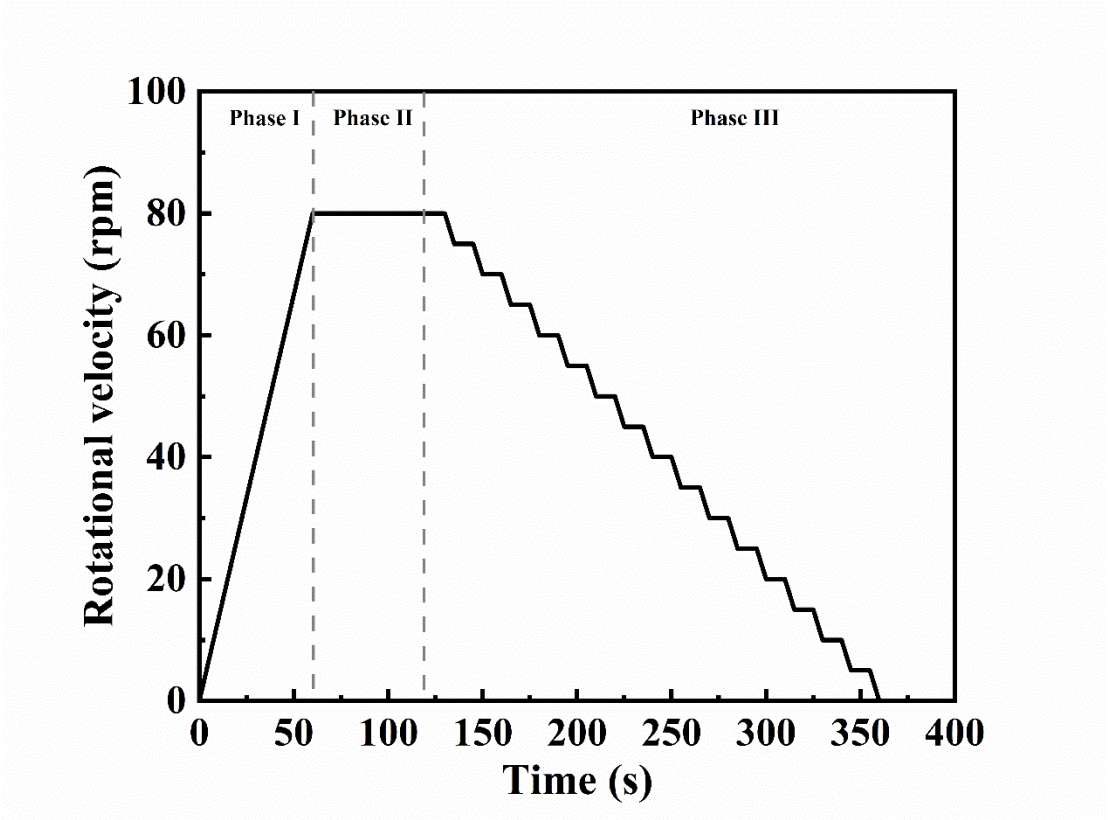

Fig. 9 Rheological test regime for measuring rheological parameters of pastes (Phase I: increased velocity stage. Phase II: constant velocity stage, i.e., pre-shearing stage. Phase III: testing stage)

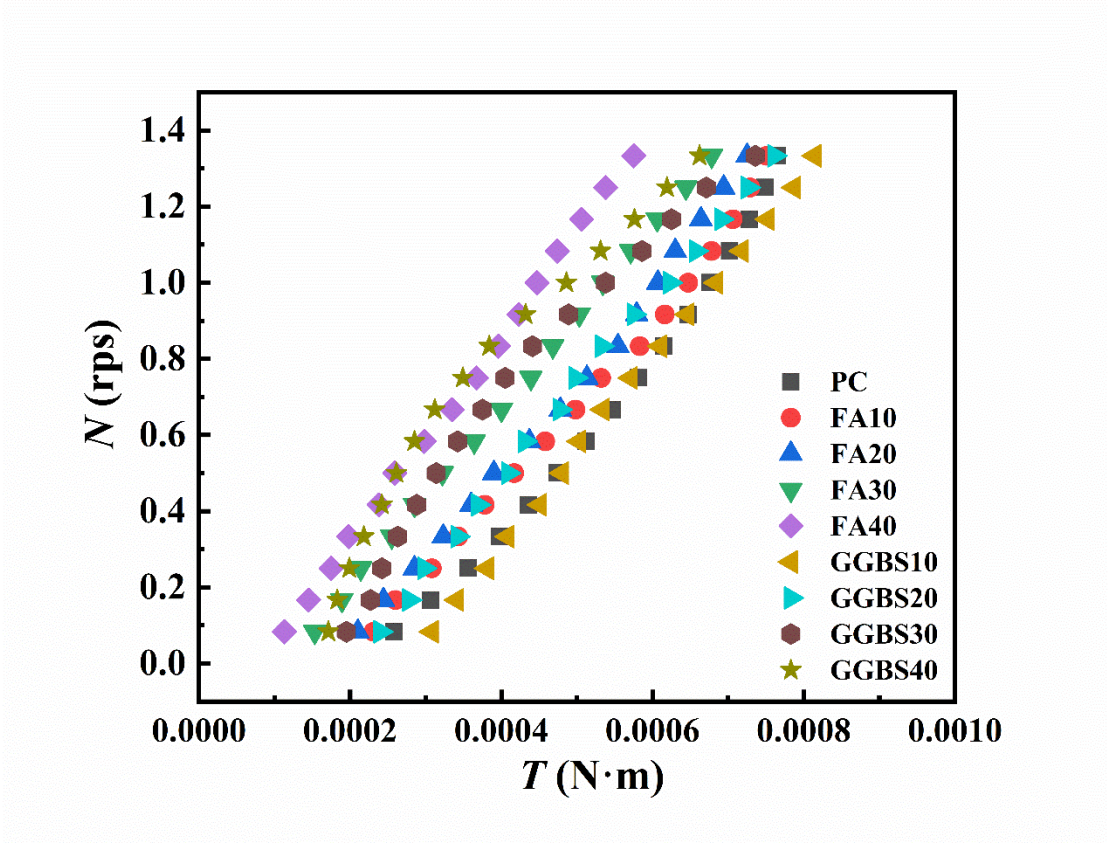

(a)

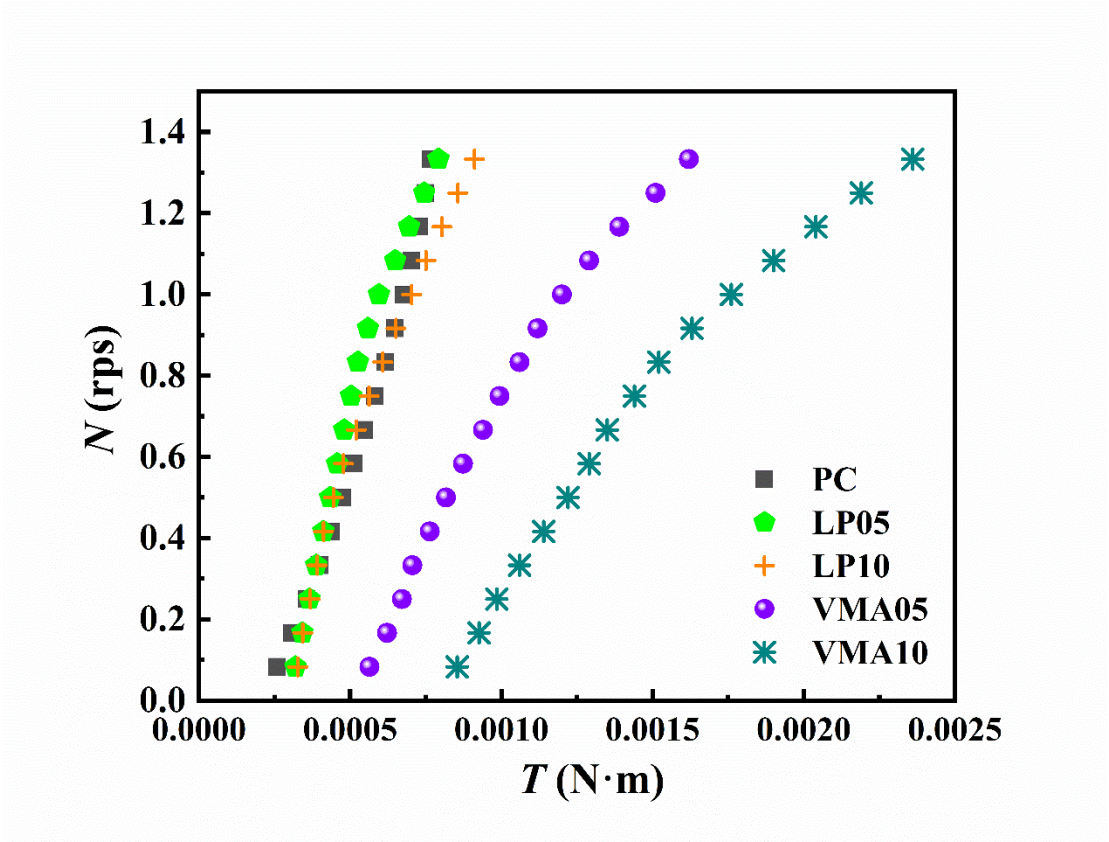

(b)

Fig. 10 *N*-*T* points of fresh pastes under different mix proportions

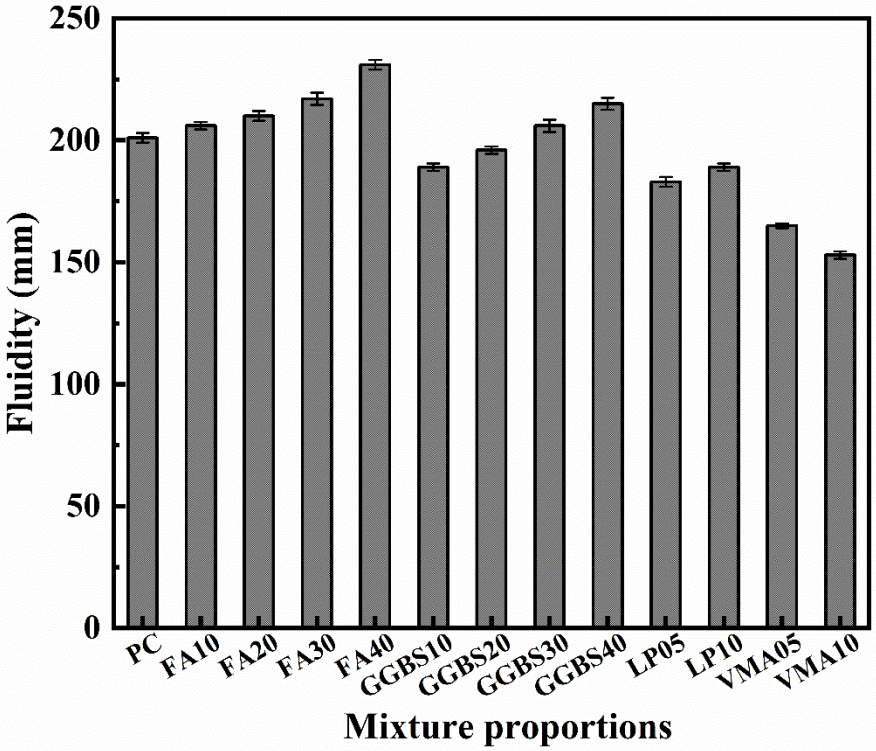

Fig. 11 Effect of admixtures on fluidity of fresh pastes

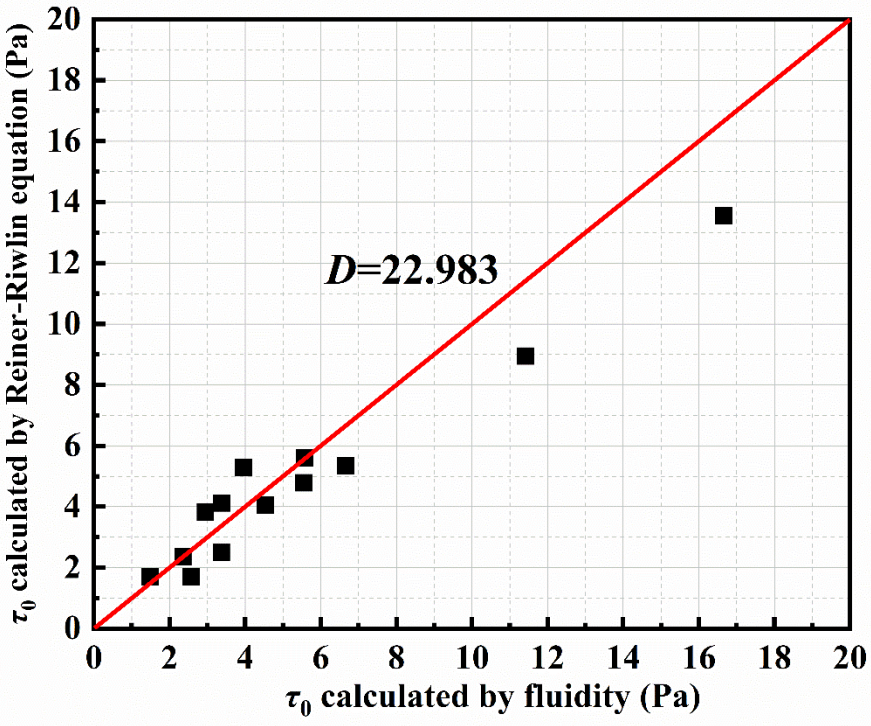

(a)

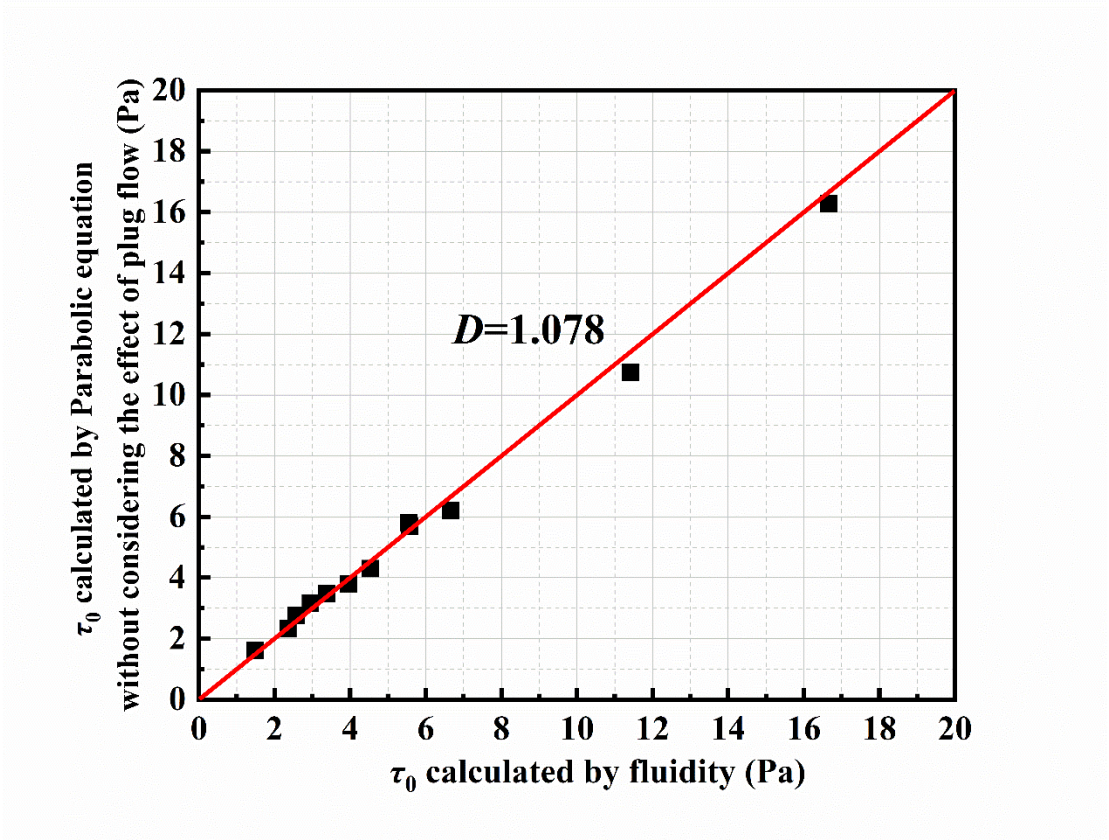
τ_0 calculated by Parabolic equation
without considering the effect of plug flow (Pa)
τ_0 calculated by fluidity (Pa)
D=1.078
0
2
4
6
8
10
12
14
16
18
20

(b)

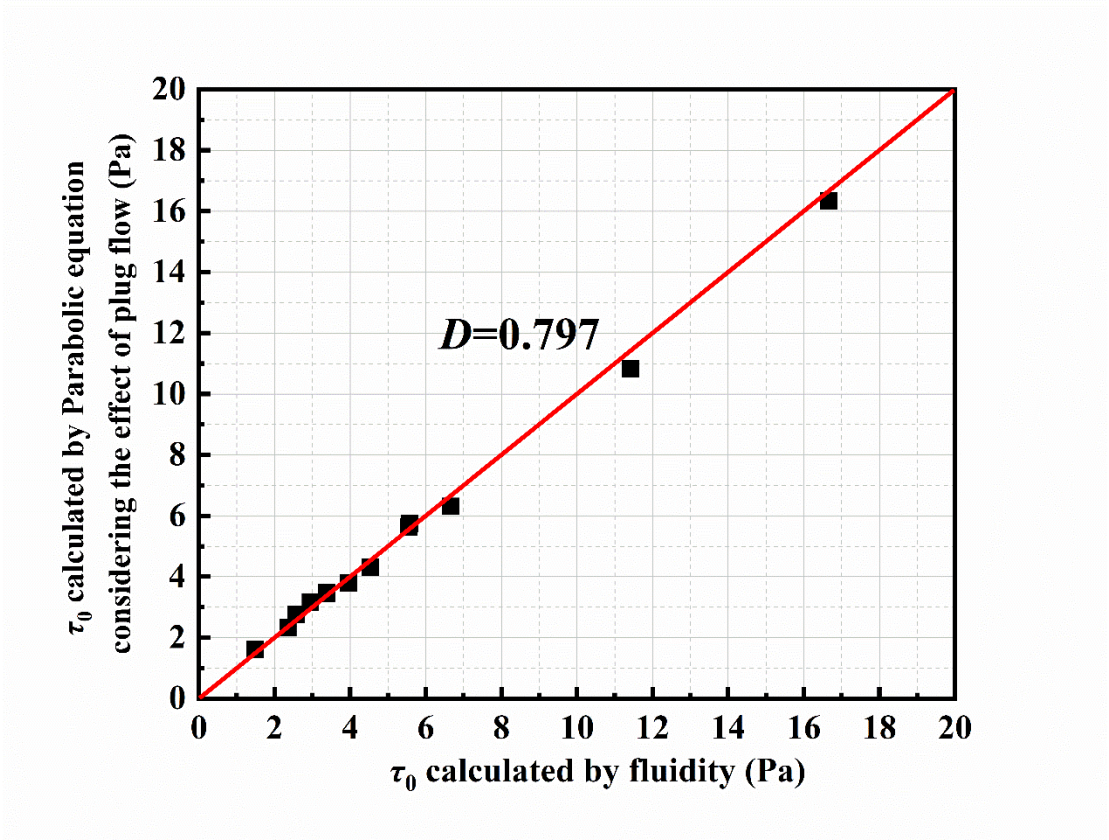

(c)

Fig. 12 Comparison of yield stress obtained by different theoretical calculation methods and yield stress obtained by mini-cone slump test, showing (a) τ_0 calculated by fluidity *vs.* τ_0 calculated by Reiner–Riwlin equation, (b) τ_0 calculated by fluidity *vs.* τ_0 calculated by the Parabolic model without considering the effect of plug flow, and (c) τ_0 calculated by fluidity *vs.* τ_0 calculated by the Parabolic model considering the effect of plug flow

Table 1 Chemical compositions and physical properties of cementitious materials

Raw materials	Content (%)							Loss on ignition (%)	Specific surface area (m^2/kg)	Density of cementitious materials (g/cm^3)
	SiO_2	Al_2O_3	Fe_2O_3	CaO	MgO	SO_3	f-CaO			
PC	20.8	7.3	3.3	62.3	2.9	2.8	0.7	2.1	367	3.15
FA	52.7	25.8	9.7	3.7	1.2	0.2	-	4.2	484	2.45
GGBS	26.1	13.8	14.2	33.6	8.1	-	-	3.6	450	2.87
LP	1.2	0.6	0.2	56.3	0.4	-	-	-	573	2.63

Table 2 Mix proportions of pastes prepared in this study (g)

No.	Sample	PC	FA	GGBS	LP	VMA	Water	PCE
1	PC	500	0	0	0	0	150	1.5
2	FA10	450	50	0	0	0	150	1.5
3	FA20	400	100	0	0	0	150	1.5
4	FA30	350	150	0	0	0	150	1.5
5	FA40	300	200	0	0	0	150	1.5
6	GGBS10	450	0	50	0	0	150	1.5
7	GGBS20	400	0	100	0	0	150	1.5
8	GGBS30	350	0	150	0	0	150	1.5
9	GGBS40	300	0	200	0	0	150	1.5
10	LP05	475	0	0	25	0	150	1.5
11	LP10	450	0	0	50	0	150	1.5
12	VMA05	475	0	0	0	25	150	1.5
13	VMA10	450	0	0	0	50	150	1.5

Table 3 Determination of plug flow in process of calculating the yield stress of pastes under different mix proportions (√: plug flow exists, i.e., $\tau_{min} < \tau_0$. ×: plug flow does not exist, i.e., $\tau_{min} > \tau_0$.)

Sample	1	2	3	4	5	6	7	8	9	10	11	12	13
Point 1~Point 16	×	×	×	×	×	√	√	√	×	√	√	√	√
Point 2~Point 16	×	×	×	×	×	×	×	×	×	√	×	×	×
Point 3~Point 16	×	×	×	×	×	×	×	×	×	×	×	×	×